machines

MDPI

Article

Study on Temperature Field Uniformity of Dynamic Induction Heating for Camshaft of Marine Diesel Engine

Xiaona Shi, Kelong Wang, Guochao Li, Chenghao Lyu, Lei Zhao *, Jianzhi Chen, Li Sun and Hengheng Wu

School of Mechanical Engineering, Jiangsu University of Science and Technology, Zhenjiang 212003, China; shixn@just.edu.cn (X.S.); 18843301995@163.com (K.W.); liguochao@just.edu.cn (G.L.); lch1528928491@126.com (C.L.); jzchen@just.edu.cn (J.C.); sunl@just.edu.cn (L.S.); wuhengheng@just.edu.cn (H.W.)
* Correspondence: zhaogoe@just.edu.cn; Tel.: + 86-130-0987-3356

Abstract: This paper focuses on the study of the induction heating process of a camshaft in a marine diesel engine. A three-dimensional finite element model for dynamic induction heating is established using the finite element method of multi-physical field coupling, aiming to investigate the temperature uniformity of the cam during this process. Three elements are analyzed in this study: the moving speed, the gap between the induction coil and the workpiece, and the width of the induction coil. These factors allow for an analysis of the temperature distribution in the thickness direction and contour line direction of the cam under various conditions. On this basis, an equivalent parameter about the temperature uniformity in the thickness direction of the cam is proposed to guide the selection of the camshaft induction heating process parameters.

Keywords: camshaft; induction heating; dynamic; temperature uniformity; equivalent parameters

check for updates

Citation: Shi, X.; Wang, K.; Li, G.; Lyu, C.; Zhao, L.; Chen, J.; Sun, L.; Wu, H. Study on Temperature Field Uniformity of Dynamic Induction Heating for Camshaft of Marine Diesel Engine. *Machines* **2024**, *12*, 215. https://doi.org/10.3390/machines12040215

Academic Editor: Davide Astolfi

Received: 14 February 2024
Revised: 21 March 2024
Accepted: 21 March 2024
Published: 23 March 2024

Copyright: © 2024 by the authors. Licensee MDPI, Basel, Switzerland. This article is an open access article distributed under the terms and conditions of the Creative Commons Attribution (CC BY) license (https://creativecommons.org/licenses/by/4.0/).

1. Introduction

As a key part of a marine diesel engine, the camshaft plays a role in controlling the cylinder switch of the diesel engine in actual operation. Due to the harsh working environment of the camshaft, high relative motion speed, and cam and tappet contact force complexity; this results in serious wear of the cam working surface, as shown in Figure 1. The induction hardening process causes a significant temperature differential between the different regions of the cam because of the intricate contour line of the cam, the influence of the skin effect, and the end effect. It is easy to lead to the emergence of problems such as the uneven distribution of soft bands and hardened layers. This poses a significant challenge to the wear resistance of the camshaft and detrimentally impacts the longevity and performance of the diesel engine.

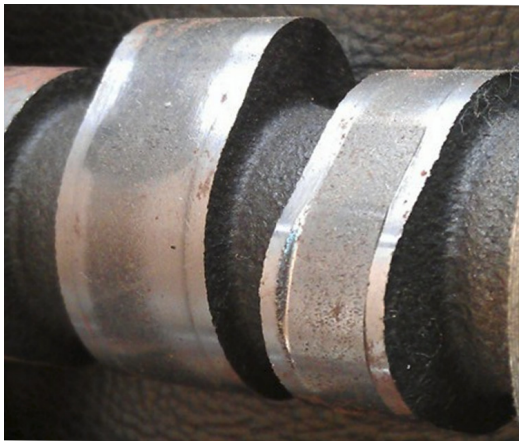


Figure 1. Cam wear.

Induction hardening is a surface-strengthening technology that has the characteristics of fast heating speed and high efficiency. At the same time, the surface hardness that can be achieved is higher, and it is easier to meet the needs of actual production. In recent years, due to the many advantages of induction hardening, the use of induction hardening in the industry has increased [1,2]. Induction hardening can produce a hardened layer on the surface of the workpiece to achieve the purpose of improving the surface properties, such as wear resistance and hardness of the workpiece [3]. However, as an important component of induction hardening, the quality of induction heating directly affects the surface properties after induction hardening [4]. Therefore, it is meaningful to study the distribution of temperature fields and the influence factors of temperature uniformity under different factors in the induction heating process.

Since the object of this paper is the camshaft of a marine diesel engine, the overall size of the camshaft is relatively large. It is costly to experimentally study the temperature distribution and the influencing factors of the cam in the induction heating process. However, with the gradual maturity of computer simulation technology, its efficiency, safety, and reliability are constantly improved. The finite element software is used to simulate the induction heating or induction hardening process of the workpiece, which more intuitively shows the distribution of temperature, magnetic field, and residual stress during the machining process. This greatly reduces the cost of cam induction heating technology research. At the same time, finite element technology can not only simulate the experimental process to obtain similar experimental results. It can also predict the experimental results based on the simulation results [5]. Therefore, more and more scholars are adopting finite element simulation technology in the study of time-induction hardening technology [6–8].

A crucial step in the induction hardening process is induction heating; the workpiece's surface strengthening characteristics are directly impacted by the heating quality of the process, and the hardened layer formation and the distribution's surface qualities play a major role [9,10]. In recent years, the study of temperature uniformity during induction heating has attracted the attention of many researchers. Huiping Li et al. [11] found that the uneven distribution of heating temperatures will lead to uneven hardness. M. Fisk et al. [12] used finite element software to simulate the rapid induction heating process. It was found that the heating speed and the peak temperature of the workpiece had a great influence on the depth of the hardened layer. Transverse flux induction heating usually places the conductor inside the coil, and the direction of the magnetic flux generated by the induction coil is perpendicular to the heated surface. The purpose of longitudinal flux induction heating heat the metal by letting the direction of the magnetic flux parallel to the heated surface and generating an induced current inside the metal. Wen Peng et al. [13] established a finite element model of transverse flux induction heating, considering the influence of magnetic shielding on temperature uniformity, and improved the temperature uniformity by optimizing the combination of magnetic shielding. Yu C et al. [14] showed that transverse flux induction heating can effectively heat the slab surface between continuous casting and hot rolling compared with longitudinal flux heating, and selecting appropriate parameters can make the temperature distribution more uniform. WU Y et al. [15] explored the relationship between the structure of the induction coil and the temperature field distribution and found that the uniformity of the temperature distribution can be improved by changing the number of turns of the coil. Song K. J. et al. [16] studied the relationship between the coil structure and the temperature field and believed that the uneven temperature distribution is caused by the center effect and the end effect. The variable radius can effectively reduce the axial temperature difference and improve the heating efficiency. Peng C et al. [17] proposed a focused induction heating method that realized temperature control in the induction heating process on the basis of improving heating efficiency. By providing current with different frequencies and adjusting the distribution of temperature, the temperature uniformity of the research object could be improved, and a good distribution of hardened layers could be obtained [18–20]. Iterative heating is improved and optimized on the basis of induction

heating technology, and the surface strengthening quality is improved by multiple heating of the workpiece. Zhao Y et al. [21] explored the influence of dual-frequency induction heating process parameters on temperature distribution under multiple iterative heating. The research results showed that with the increase in the number of iterations, the uniformity of the temperature distribution on the surface of the workpiece continuously improved. Feng Li et al. [22] used the finite element method to study planar induction heating (a technique for heating a metal plane using the principle of electromagnetic induction), considering the correlation between material properties and temperature. Kai Gao et al. [23] found that the temperature uniformity is affected by the feed path and the shape of the workpiece by studying the Induction hardening of the curved surface, and the uniformity of the temperature distribution is relatively reduced with the increase in curvature. The researchers mentioned above focus primarily on process factors, inductor structure, material qualities, and induction heating when examining the uniformity of temperature improvement. In the actual production situation, some processes are dynamic, so the motion factor cannot be ignored. In order to reduce the problem of excessive temperature in the middle of the cam and more accurately represent the process of cam induction heating, it is necessary to introduce mobile induction heating. SAPUTRO I E et al. [24] studied large spur gears and analyzed the influence of scanning speed and air gap on the hardened layer of gears. The reduction of scanning speed and air gap can improve the problem of insufficient hardened layers. Huaiyu W. et al. [25] studied the evolution of the end temperature of the gear during induction heating and found that the hysteresis distance of the end temperature is proportional to the scanning speed within a certain range, which provides a basis for improving the heating quality of the end position. There are relatively few studies on mobile induction heating, mainly by changing the scanning speed and air gap to study the influence of temperature distribution.

There is relatively more work on simulating induction heating or induction hardening processes. However, relatively less work has been carried out for cams. In the process of induction hardening or induction heating of the cam, there will inevitably be overheating to produce cracks [26], or underheating, which makes it easy to form soft bands. This poses a huge challenge to the surface performance of the cam's working face. In actual production, the cam working surface has the highest degree of wear and failure area. Considering the heat uniformity in the induction heating process of the cam is an important means to improve the quality of cam surface strengthening [13], and it is also the main research content of this paper. The majority of researchers have focused on induction heating technologies where the workpiece and induction coil are held in a constant relative position. The induction heating technique under motion has received relatively little research and development. However, the movement factor cannot be ignored. Adding motion factors to the cam induction heating model is exactly what this paper studies.

This paper mainly combines the dynamic numerical simulation of the camshaft movement and the establishment of a cam dynamic induction heating model. Compare the temperature distribution in the static induction heating process, study the influence factors and change rules in the dynamic situation, and analyze the causes of uneven temperature distribution on the cam surface. By adjusting the width of the profiling induction coil and other factors, the temperature difference in the thickness direction of the cam is reduced, the surface temperature distribution is improved, the uniformity of the temperature distribution is improved, and the relevant parameters in the induction heating process of the cam are optimized. It provides a corresponding reference for solving the problem of uneven temperature during the heating process of the cam.

2. Mathematical Model of Induction Heating

Induction heating is an important process for cams to obtain good heating quality. Good heating quality is the key to obtaining good surface properties of cams. For the induction heating process in this paper, the electromagnetic field and temperature field to described as two aspects.

2.1. Mathematical Model of Electromagnetic Field

The induction heating process can be described using Maxwell's equations to express the electromagnetic field. This field can be classified as a quasi-static electromagnetic field due to the wavelength of the electromagnetic wave is much larger than the size of the workpiece. In the induction heating process of this paper, the displacement current can be considered to be zero, so Maxwell 's equations can be expressed as:

$$\nabla \times H = J + \frac{\partial D}{\partial t} \tag{1}$$

$$\nabla \times E = -\frac{\partial B}{\partial t} \tag{2}$$

$$\nabla \cdot D = 0 \tag{3}$$

$$\nabla \cdot B = 0 \tag{4}$$

where H is the magnetic field intensity (A/m), D is the potential offset vector (C/m^2), J is the current density (A/m^2), E is the electric field intensity (V/m), and B is the magnetic induction intensity (T).

Solve for the intrinsic relations of the medium in the domain as:

$$D = \varepsilon E \tag{5}$$

$$B = \mu H \tag{6}$$

$$J = \sigma E \tag{7}$$

where ε is the dielectric constant (F/m), μ is the magnetic permeability (h/m), and σ is the electrical conductivity (S/m).

In order to simplify the process of solving the electromagnetic field problem and obtain the electromagnetic field and eddy current field in the induction heating process, the electric potential and vector magnetic potential are introduced into the above equations to separate the variable scalars of the electric field and the magnetic field. Define the scalar potential $\varnothing$ and the vector magnetic potential A. According to the vector analysis, the curl of any vector is calculated and then the divergence is calculated, and the value is zero. Therefore, the vector A is combined with Equation (4) to obtain the following equation:

$$B = \nabla \times A \tag{8}$$

It can be seen from Equation (8) that the magnetic induction intensity B can be expressed by the curl of vector A. The vector A defined above has no practical physical meaning in the macroscopic electromagnetic field, but only to simplify the difficulty of solving the electromagnetic field. By comparing Equation (8) with Equations (1) and (3), the following equations can be obtained:

$$\nabla \times \frac{1}{\mu} \nabla \times A = J \tag{9}$$

Substituting Equation (8) into Equation (2), the following equation is obtained:

$$\nabla \times E = -\frac{\partial}{\partial t} \nabla \times A = -\nabla \times \frac{\partial A}{\partial t} \tag{10}$$

The following equation can be obtained from Equation (10):

$$\nabla \times \left(E + \frac{\partial A}{\partial t} \right) = 0 \tag{11}$$

Since an irrotational vector field is formed in the brackets of Equation (11), the irrotational vector field can be expressed as a gradient of a scalar field, which can be expressed by the scalar potential $\varnothing$ introduced above:

$$E + \frac{\partial A}{\partial t} = -\nabla \varnothing \tag{12}$$

Therefore, Equation (12) can be changed to the following equation:

$$E = -\frac{\partial A}{\partial t} - \nabla \varnothing \tag{13}$$

By simultaneous Equations (7) and (13), the current density can be expressed as:

$$J = \sigma E = -\sigma \frac{\partial A}{\partial t} - \sigma \nabla \varnothing \tag{14}$$

Substituting Equation (14) into Equation (9), the control equation of eddy current in the induction heating process can be obtained as follows:

$$\nabla \times \left(\frac{1}{\mu} \nabla \cdot A \right) + \sigma \frac{\partial A}{\partial t} + \sigma \nabla \varnothing = 0 \tag{15}$$

In this paper, the introduction of vector magnetic potential A and the definition of scalar potential $\varnothing$ are mainly to simplify the mathematical model of the electromagnetic field. The introduction of vector magnetic potential A can transform the equation of electromagnetic field into vector form, and the definition of scalar potential can express the current density of electromagnetic field as a function of scalar form, so as to further simplify the calculation and analysis of electromagnetic field. At the same time, it can better describe the boundary conditions of the electromagnetic field.

2.2. Mathematical Model of Temperature Field

The temperature field of the cam during induction heating can be expressed by Fourier partial differential equation as follows:

$$k(T) \left(\frac{\partial^2 T}{\partial x^2} + \frac{\partial^2 T}{\partial y^2} + \frac{\partial^2 T}{\partial z^2} \right) + q_V = \rho c_p(T) \frac{\partial T}{\partial t} \tag{16}$$

where k is the thermal conductivity of isotropic material (W/m·°C); T is the instantaneous temperature (°C); ρ is the density of the material (kg/m^3); c_p is the specific heat capacity of the material (J/kg·°C); q_v is the intensity of the internal heat source (W/m^3); t is the induction heating time (s).

The boundary conditions in the temperature field are determined. The temperature boundary conditions in this paper are:

$$T = f(x, y, z, t) \tag{17}$$

Convective heat transfer and radiation boundary conditions between air and workpiece surface:

$$-\lambda \frac{\partial T}{\partial n} = h\left(T - T_f \right) \tag{18}$$

$$h_r = \varepsilon_r \sigma F_a \left(T^4 - T_f^4 \right) \tag{19}$$

where h is the surface convective heat transfer coefficient(W/m^2 °C), λ is the thermal conductivity, $\frac{\partial T}{\partial n}$ is the temperature gradient (the derivative of temperature in the n direction), n is the unit vector in the normal direction, T_f is the ambient temperature (°C), usually $T_f = 20$ °C. h_r is the radiative heat transfer coefficient, ε_r is the radiation coefficient of the surface of the material, σ is the Boltzmann's constant, $\sigma = 1.38{\cdot}10^{-23}$ (W/m$^2{\cdot}$K^4), and F_a is the angular coefficient of thermal radiation. The convective heat transfer coefficient h between air and cam surface is 100 W/(m^2 °C), and the radiative heat transfer coefficient is 0.8 [27,28].

3. Establishment of the Finite Element Model

In Section 2, the mathematical model of induction heating is analyzed from the electromagnetic field and temperature field. Based on the above analysis, the simulation model of cam induction heating is established by COMSOL Multiphysics ®6.1 software. Istardi, D. [29] and MatúšO [30] presented selected applications of the software used. However, for complex multi-physics problems, the use of finite element software is inevitably the calculation accuracy and applicability of the software itself. Kennedy, M [31] provided further verification of numerical and experimental results for the simulation results obtained by COMSOL software. LEITNER M et al. [5] simulated induction heating by COMSOL software, and further proved the applicability of the software.

For the problem of using the finite element method to realize the uniform distribution of the surface temperature of the workpiece in induction heating, many scholars have used the finite element method to study the induction heating and induction quenching process [32–34]. This gives us a good reference. It also proves the feasibility of this method. Select the appropriate meshing and optimize the grid at different positions in the model. Ensure that the calculation accuracy is not greatly affected while reducing the amount of calculation. At the same time, the selection of material properties and boundary conditions has an important influence on the calculation accuracy. In this paper, the relationship between material and temperature is considered. In the process of numerical analysis, the convective heat transfer and radiative heat transfer between the workpiece and air are also considered. At the same time, in order to simulate the actual production conditions and improve the accuracy of the model, an infinite element domain is established in the model.

Figure 2a shows the induction hardening process of camshafts in the actual production process. In this paper, COMSOL software is used to establish the finite element model of cam induction heating shown in Figure 2b. The model includes three parts: profiling induction coil, cam, and air domain. The free tetrahedral mesh is used to divide the model, and the cam and the induction coil are extremely refined. Since the cam is affected by the skin effect resulting in a large temperature difference between the surface and the interior, this paper encrypts the mesh on the surface of the cam and sets the boundary layer mesh on the surface with a number of layers of 4, a tensile factor of 1.2, a total thickness of 4 mm, and the number of mesh cells of 26,723. A graph depicting the time step on the x-axis and the reciprocal of the step on the Y-axis often illustrates the convergence of the simulation model in COMSOL software. Therefore, based on the above conditions, the convergence curve shown in Figure 3 is obtained. Figure 3 shows that as the time step increases, the time step will also automatically increase, the reciprocal of step size will also drop, and the convergence curve will exhibit a downward trend. This shows that the convergence of the model is better.

The material used for the cam is 18CrNiMo steel, and the chemical composition of 18CrNiMo steel is given in Table 1. In this paper, 18CrNiMo steel is selected based on the needs of the actual factory, and the related material properties of 18CrNiMo steel in the heating process are calculated by JmatPro 7.0 software [35–37]. The thermal conductivity, specific heat capacity, resistivity, relative permeability, and other material properties of the material change with temperature, as shown in Figure 4.

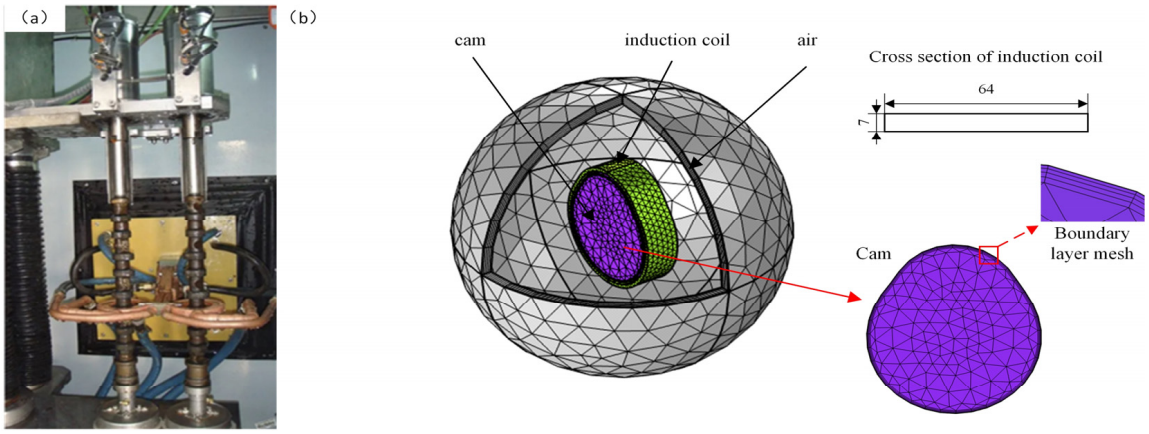


Figure 2. (**a**) Induction hardening of camshaft; (**b**) Simulation model of the cam.

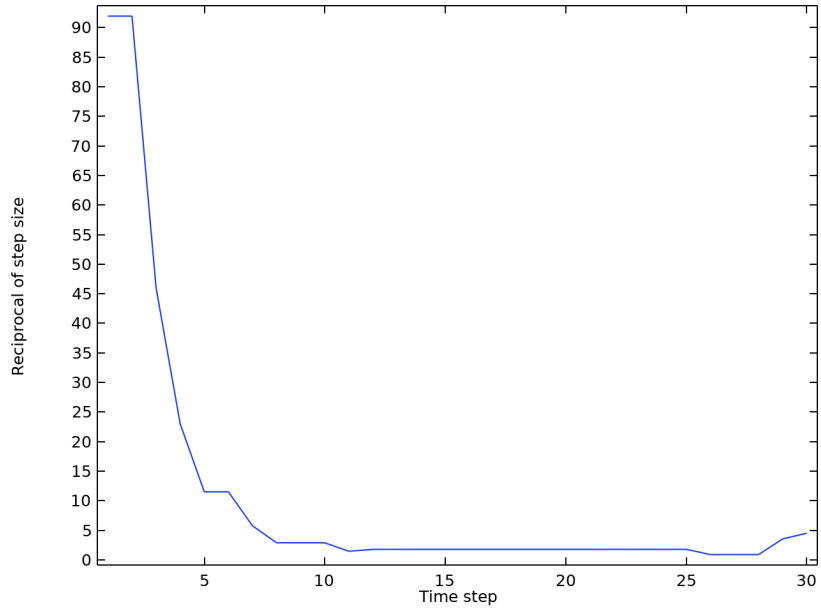


Figure 3. Convergence curve of the simulation model.

Table 1. Chemical composition of 18CrNiMo steel (mass fraction, %).

C	Si	Mn	Ni	P	S	Cr	Mo
0.15~0.21	≤0.4	0.5~0.9	1.4~1.7	≤0.025	≤0.035	1.5~1.8	0.25~0.35

Since the research in this paper is dynamic induction heating, the motion factor of cam translation is added to the above model. Thus, a frequency domain-transient simulation model is established. The following is the specific setting of the simulation model.

The initial conditions of the finite element model for dynamic induction heating are as follows: the current frequency is set to 8000 Hz, the current is set to 760 A, the coil material is pure copper, the width is 64 mm, the coil is uniformly multi-turn, with 15 turns total, and the coil type is set to numerical type. The initial gap between the induction coil and the workpiece is 5 mm, the initial motion speed of the cam is v = 10 mm/s, the heating time is 15s, and the initial temperature of the workpiece and the ambient temperature are both 293.15 K. Considering the convective heat flux, the heat transfer coefficient is 100 W/(m^2·K), and the radiant heat transfer coefficient is 0.8. The size of the cam model is shown in Figure 5. The thermal conductivity, specific heat capacity, resistivity, relative permeability, and other related material properties of the cam material are calculated by

Jmatpro software and input into the finite element model to obtain the dynamic induction heating temperature result of the cam as shown in Figure 6.

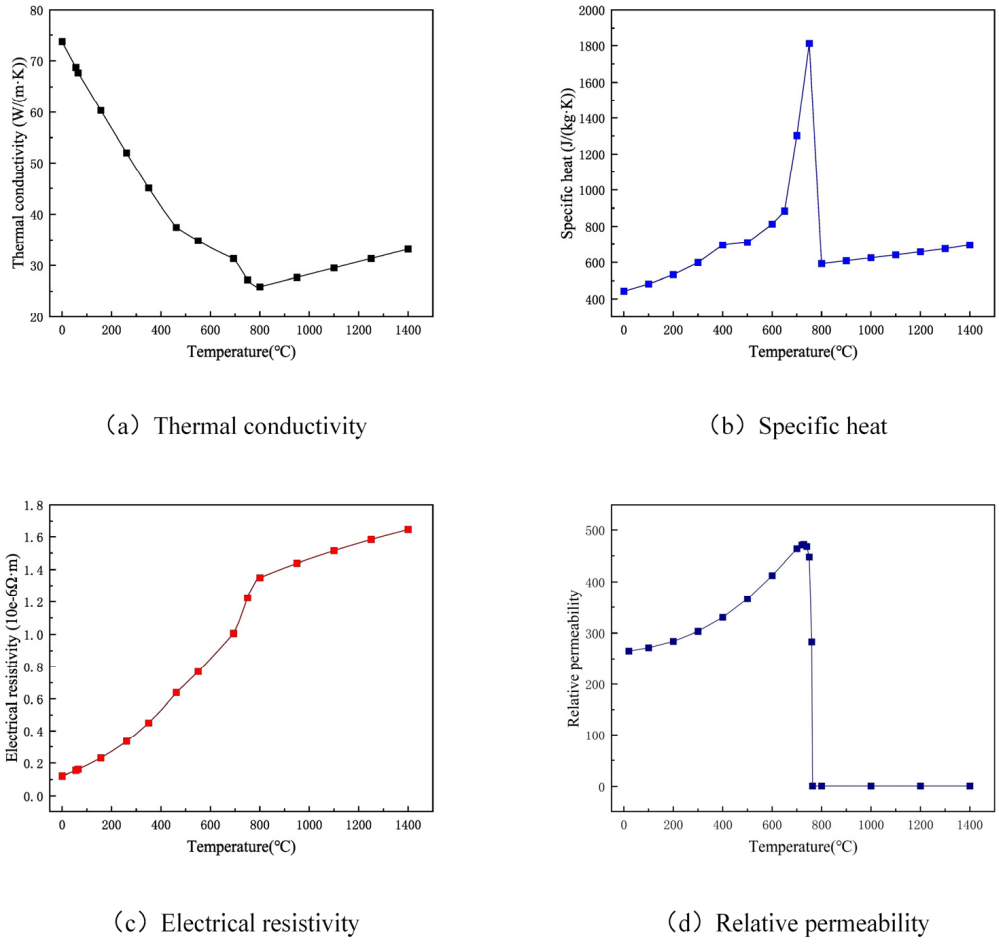


Figure 4. Material property parameters of 18CrNiMo steel: (**a**) Thermal conductivity; (**b**) Specific heat; (**c**) Electrical Resistivity; (**d**) Relative permeability.

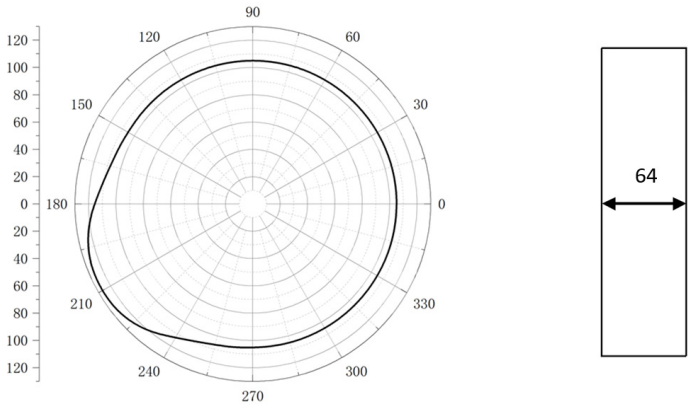


Figure 5. Cam polar plot.

In this paper, the finite element simulation method is used to calculate the multi-physical field coupling of cam induction heating by COMSOL software. Compared with static induction heating, the temperature distribution of the cam under dynamic induction heating is studied. Using temperature difference as the evaluation standard of temperature uniformity, the uniformity of temperature distribution in the thickness direction and contour direction of the cam is analyzed, and the influence of different factors on

temperature uniformity is discussed. The equivalent relationship between temperature and other parameters in the thickness direction of the cam is proposed. This paper discusses three process factors: cam moving speed, coil and workpiece gap, and induction coil width. Through the control variable method, the value of one variable is changed each time, to explore the change of temperature uniformity of the three variables under different values. The values of the three variables are shown in Table 2.

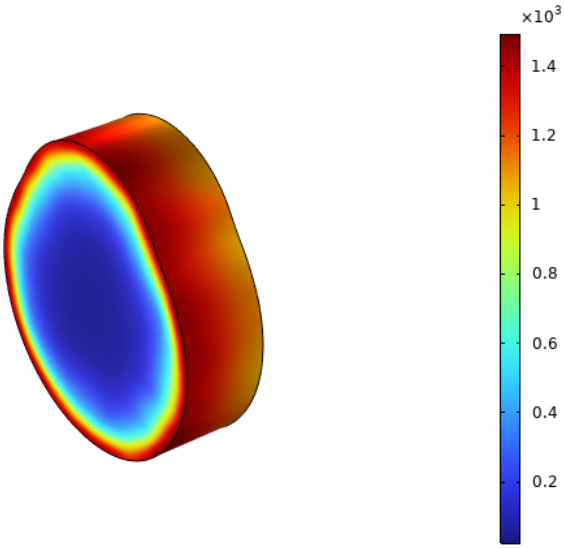


Figure 6. Temperature field distribution.

Table 2. Value of different process factors.

Serial Number	Moving Speed (mm/s)	Gap (mm)	Induction Coil Width (mm)	Serial Number	Moving Speed (mm/s)	Gap (mm)	Induction Coil Width (mm)
1	5	5	64	13	10	3	64
2	6	5	64	14	10	4	64
3	7	5	64	15	10	5	64
4	8	5	64	16	10	6	64
5	9	5	64	17	10	7	64
6	9.25	5	64	18	10	8	64
7	10	5	64	19	10	5	16
8	11	5	64	20	10	5	32
9	12	5	64	21	10	5	48
10	13	5	64	22	10	5	64
11	14	5	64	23	10	5	80
12	15	5	64				

4. Results and Analysis

4.1. Static Induction Heating

The initial state of the static induction heating model is depicted in Figure 2, with the induction coil and cam kept motionless. The heating process is then continued for 15 s. When the movement speed is zero, the impact of the cam's temperature distribution during the heating process is investigated.

Figure 7 shows the change of the surface temperature of the cam with the heating time during the static induction heating process, and gives the change and distribution of the temperature of the cam during the whole heating process. The figure shows that after two seconds, the temperature in the middle of the cam begins to rise significantly. As the heating time increases, the temperature progressively moves from the middle to the two ends of the cam. In this research, a wide contour cam is the focus of investigation. The cam thickness is large, the temperature decreases in outward conduction due to the factor of

heat transfer coefficient, and there is a large temperature difference between the cams in the thickness direction. Due to the complex contour of the cam and the structure of the induction coil, the temperature of the cam in the transition area is significantly lower than that in other parts, and the soft belt appears.

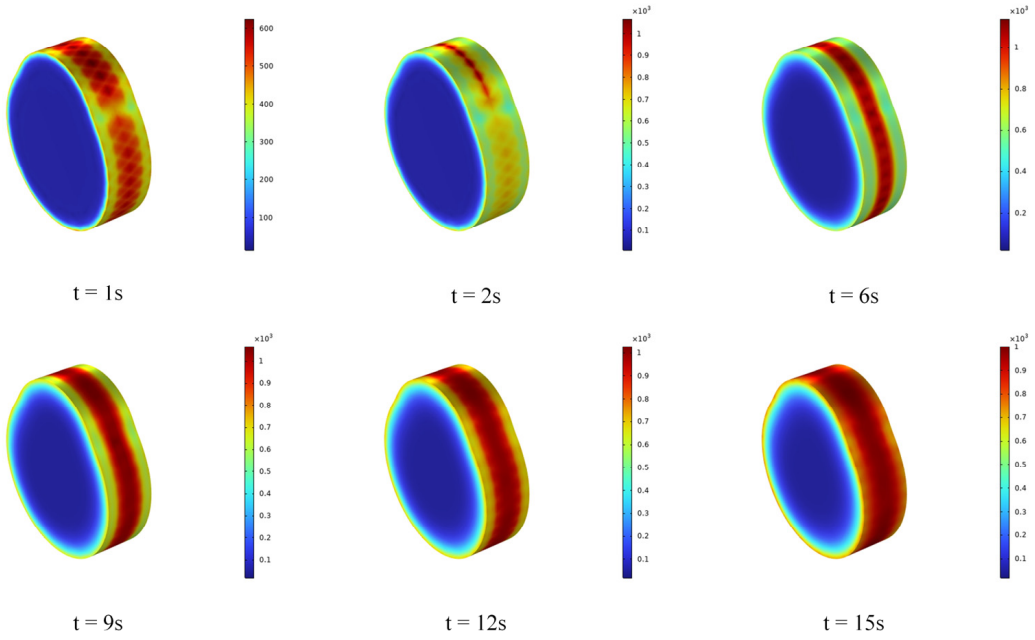


Figure 7. Cam surface temperature distribution (°C).

Figure 8 shows the distribution of magnetic flux density mode under different heating times, the profiling induction coil makes the magnetic field line of induction heating mainly gather to the middle part. With the increase of time, the dense area of the magnetic field line diffuses to both ends, and the magnetic flux density mode at both ends of the cam is smaller than that at the middle part. When t = 2s, the middle portion of the cam reaches the Curie point of the material. This results in a dramatic decrease in the magnetic flux density and a change in the material's properties from ferromagnetic to paramagnetic, with the relative permeability of the cam's middle position becoming 1. As time progresses, the entire surface of the cam, excluding the transition area, also reaches the Curie point. Consequently, the majority of the cam surface becomes the demagnetization area, leading to a significant decrease in the overall magnetic flux density.

A rectangular coordinate system is established at the top of the cam, as shown in Figure 9a. Points along the x-axis are selected to analyze the temperature distribution in the cam's thickness direction as the x-axis increases. The temperature change over time for x = 0 mm, 16 mm, 32 mm, 48 mm, and 64 mm is depicted in Figure 9b. The figure shows that as heating time increases, the overall temperature first rises dramatically before tending to stabilize. Since the dense area of magnetic lines is mainly concentrated in the middle of the cam, the temperature rises faster at x = 32 mm (the midpoint of the cam thickness) and reaches a maximum temperature of 1112 °C. The overall temperature distribution is symmetrical about x = 32 mm and gradually decreases to both ends. The maximum temperature that can be reached at both ends of the cam is 744 °C, which is less than the phase transition temperature *Ac3* of the material. As a result, there is no metal phase transition and the intended hardening effect could not be achieved.

The typical position of the cam is analyzed at x = 32 mm, as shown in Figure 10, and the temperature distribution at different positions of the cam cross-section contour is analyzed. From the figure, it can be found that the temperature in the peach tip part of the cam rises faster, with a maximum temperature of 1112 °C. The temperature at point B in the transition area is low compared to other locations, and the temperature rise rate is slow, which makes it easy to produce soft bands here.

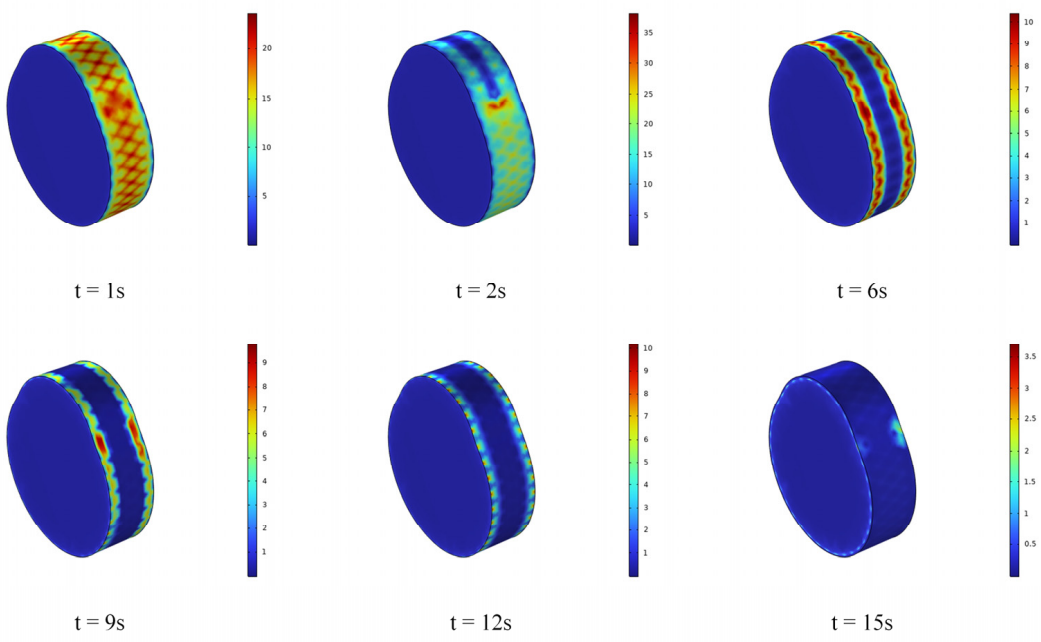


Figure 8. Magnetic flux density mode distribution on cam surface (T).

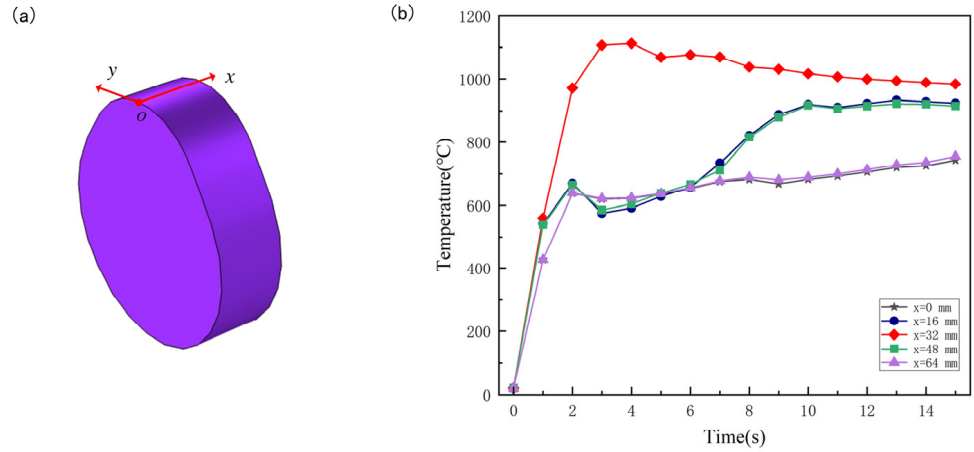


Figure 9. (**a**) Rectangular coordinate system of cam; (**b**) Temperature distribution along the *x*-axis.

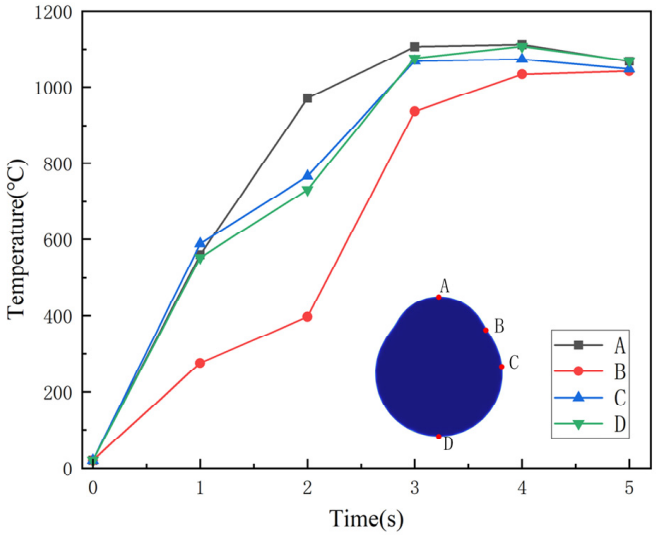


Figure 10. Temperature distribution of cam surface (A, B, C, D).

4.2. Dynamic Induction Heating

The purpose of studying the dynamic process of cam induction heating is to weaken the phenomenon of excessive temperature in the middle due to the concentration of magnetic lines during static induction heating, as well as to address issues such as slow heating rates at both ends. The objective is to improve the uniformity of the cam surface temperature.

Using the foundation of static induction heating, dynamic induction heating modifies the starting distance between the induction coil and the cam. This distance is fixed at 6 mm, as shown in Figure 11. Under the condition that the movement speed v = 10 mm/s, the temperature distribution law and the uniformity transformation in the cam induction heating process are investigated.

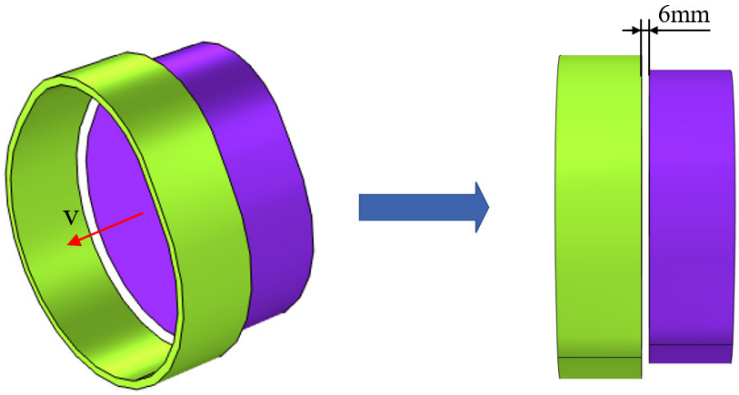


Figure 11. The initial distance between the induction coil and the workpiece under dynamic conditions.

Figures 9 and 10 show the temperature change over time during static induction heating in both the contour line direction and cam thickness direction. The magnetic force line is primarily concentrated in the center of the profiling induction coil during the static induction heating process. The temperature rise rate at this position is higher than that at the ends, resulting in uneven temperature distribution in the thickness direction of the cam. Further, dynamic induction heating of the cam is studied to analyze the temperature distribution in the thickness direction as well as on the surface of the cam.

Figure 12 shows the evolution process of the cam temperature during the dynamic induction heating process. The left end of the cam is initially heated, and over time, the heated portion gradually progresses towards the right end. Temperature distribution at six different time points is chosen to capture the evolutionary process of dynamic heating. When compared to Figure 7, it becomes apparent that dynamic induction heating significantly mitigates the issue of excessive concentration of magnetic lines in the middle section of the cam, ultimately resulting in a more uniform temperature distribution on its surface.

The temperature change of the cam along the x-axis direction with time is shown in Figure 13a. As the cam moves to the left along the axial direction, the temperature rises sharply first, and then the temperature gradually tends to be gentle after reaching a certain value. At the same time, the maximum temperature that can be reached steadily decreases as the x-axis increases in the cam's thickness direction. When x = 0 mm, the maximum temperature is 1388.8 °C, and when x = 64 mm, the minimum temperature is 1092.2 °C, and the maximum temperature difference is 296.6 °C. As the cam moves, heat is transferred from the high-temperature area to the low-temperature area. Due to some resistance to this heat transfer, the speed at which heat is transferred to the low-temperature area is slowed down, so it will lead to the direction of the thickness of the cam showing a decreasing trend in temperature. From Figure 13b, it can be seen that the cam temperature first rises sharply and then tends to be stable with the increase of heating time. The temperature changes of points A, B, C, and D with time at the cross-section of x = 32 mm in Figure 13b. It is easy to see that the temperature rise trend of the four points is consistent, and the

maximum temperature difference is not large. At the same time, the maximum temperature difference of different points on the cam contour line is only 34.1 °C. Compared with the static heating method shown in Figure 10, in the case of dynamic induction heating, the temperature distribution on the surface of the cam is more uniform, and the heating rate of point *B* is greatly improved, which reduces the possibility that the cam produces a soft belt in the transition region, and can further improve the surface strengthening quality of the cam surface.

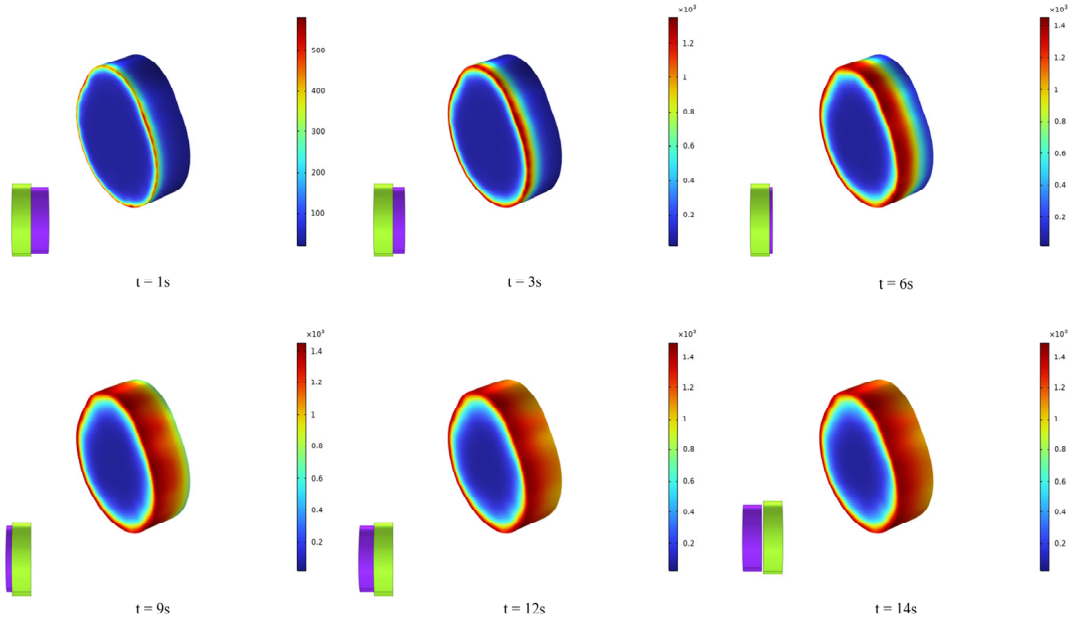


Figure 12. Temperature distribution during dynamic induction heating.

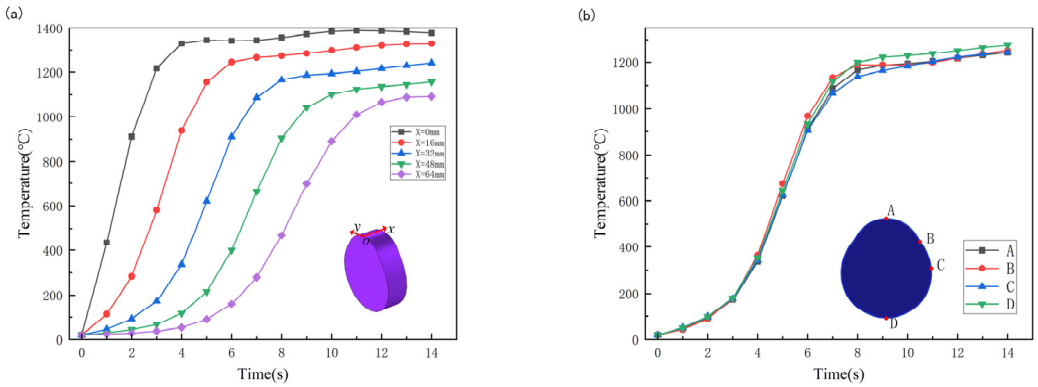


Figure 13. Temperature distribution over time during dynamic induction heating (**a**) shows the temperature distribution in the *x*-axis direction (**b**) shows the temperature distribution of the cam contour at x = 32 mm.

4.3. The Influence of Different Factors on Temperature Uniformity

In this section, the moving speed of the cam, the gap between the induction coil and the workpiece, and the width of the induction coil are discussed, respectively. The influence of the above three factors on the temperature uniformity of the cam during the dynamic induction heating process is studied, which provides theoretical support for the process optimization of the induction hardening of the cam.

4.3.1. Moving Speed

First, investigate the influence of the cam's movement speed on temperature uniformity. Figure 14 shows the relationship between the temperature difference of the cam at

different moving speeds. The curve (a) describes the relationship between the moving speed and the temperature difference in the thickness direction of the cam *A* point. The temperature difference in the thickness direction exhibits a tendency of first dropping and then increasing as the movement speed increases. The temperature difference gradually decreases as the speed ranges from 5 mm/s to 12 mm/s. At a speed of 6 mm/s, the maximum temperature difference recorded is 383 °C. Conversely, at a speed of 12 mm/s, the minimum temperature difference is 269.1 °C, indicating a decrease of 113.9 °C. The temperature distribution in the thickness direction is more uniform. When the moving speed is too slow, the heating time of the cam end is too long, which makes the temperature of the end too high. Therefore, the temperature difference in the thickness direction of the cam gradually decreases with the increase of the moving speed. When the speed is greater than 12 mm/s, the temperature difference gradually increases and the uniformity of temperature becomes worse. When the speed exceeds a certain value, the excessively fast movement speed results in a shorter dwell time of the cam in the heating zone, thus preventing it from fully absorbing energy. This leads to an uneven distribution of surface temperature on the cam, thereby reducing temperature uniformity. Curve (b) shows the relationship between the temperature difference of the x = 32 mm cross-section contour and the moving speed. The temperature difference of the cam in the contour line direction increases with the increase of the moving speed. The minimum temperature difference is 24.5 °C when the speed is 5 mm/s, and the temperature difference gradually increases with the increase of the moving speed, up to 133.6 °C.

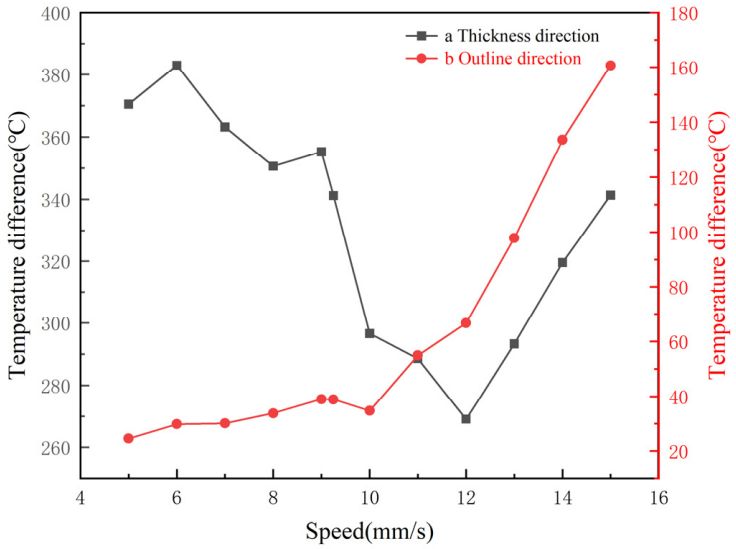


Figure 14. The variation of cam temperature difference at different moving speeds.

4.3.2. Gap between Induction Coil and Workpiece

The gap between the workpiece and the induction coil is crucial for maintaining temperature consistency during heating. A gap that is too big can cause excessive magnetic loss and lower heating efficiency, while a gap that is too small can cause workpiece damage from overheating. As a result, several gaps ranging from 3 to 8 mm are chosen in order to investigate the temperature uniformity. Figure 15 shows the variation of cam temperature difference with a gap in the thickness direction as well as in the cross-sectional contour. As shown in curve (a), the temperature difference in the thickness direction of the cam increases with the increase of the gap, and the uniformity gradually decreases. When the gap is 5 mm, the minimum temperature difference is 296.6 °C, and when the gap is 8 mm, the maximum temperature difference is 326.5 °C. The curve (b) is the temperature difference curve of the x = 32 mm section contour. With the increase of the gap, the temperature difference decreases first and then increases. When the gap is between 3–5 mm, the temperature difference gradually decreases with the increase of the gap, reach-

ing a minimum temperature difference of 34.7 °C. When the gap is greater than 5 mm, the temperature difference gradually increases, reaching a maximum temperature difference of 68.8 °C at 8 mm.

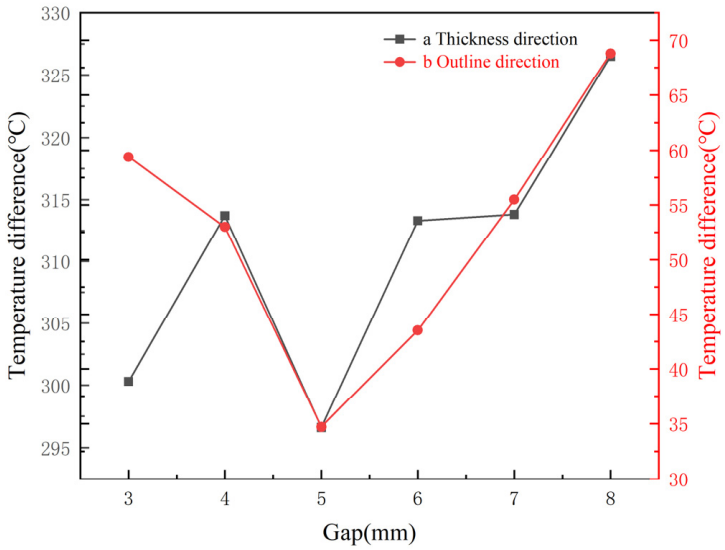


Figure 15. The variation of cam temperature difference under different clearances.

4.3.3. Width of Induction Coil

This section studies induction coils with different widths. Figure 16 shows five different widths of induction coils with widths of 64 mm (equal-width induction coil), 32 mm (1/2 induction coil), 16 mm (1/4 induction coil), 48 mm (3/4 induction coil), and 80 mm (over-thick induction coil). By simulating the induction heating process, the influence of coil width on the direction of cam thickness and the temperature at different points of the cross-section is investigated in the case of dynamic heating. In order to minimize the end effect, the initial position of the coil and the workpiece is set to 6 mm, so that the workpiece and the coil are away from each other.

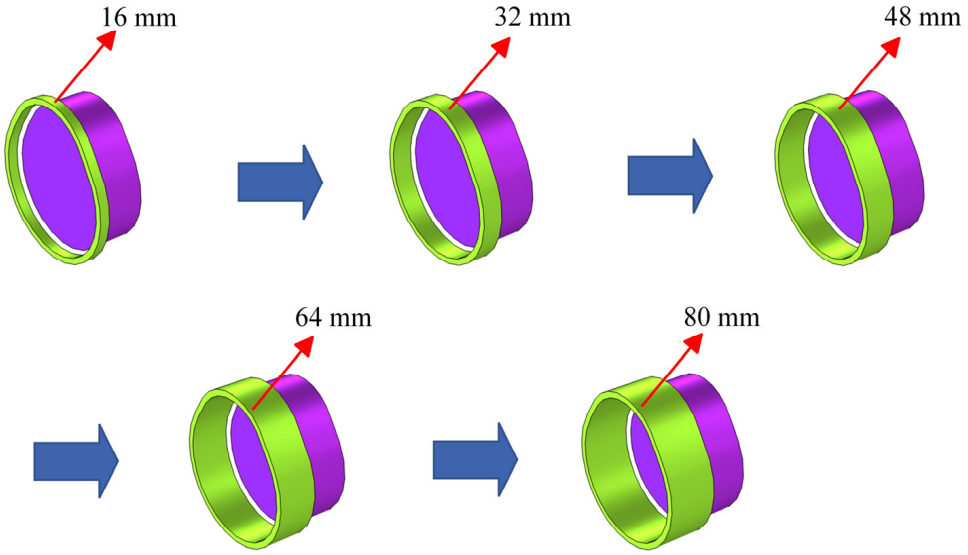


Figure 16. Size diagram of the induction coil.

The temperature differential of the cam under various induction coil widths is depicted in Figure 17. The curve (a) in the figure shows that the temperature difference in the thickness direction of the cam steadily reduces as the width of the induction coil increases. The temperature difference decreased from 401.2 °C to 262.7 °C. The reduction in the width

of the induction coil makes the electromagnetic field more concentrated, the electromagnetic field varies more in the direction of the cam thickness, and the temperature difference at different positions on the cam surface increases. Increasing the coil width can effectively reduce the temperature difference in the thickness direction of the cam and improve the uniformity of the temperature distribution. Curve (b) shows the relationship between the temperature difference of the cross-section contour of x = 32 mm and the width of the induction coil. From the figure, it can be seen that the temperature difference first fluctuates in a certain range and then rises rapidly. When the width is 48 mm, the minimum temperature difference is 23.2 °C. When the coil width is 80 mm, the temperature difference reaches the maximum of 97.4 °C. It can be seen that the width of the coil has a certain influence on the temperature distribution in the direction of the cam contour line, and the selection of an appropriate coil width is conducive to improving the uniformity of temperature distribution.

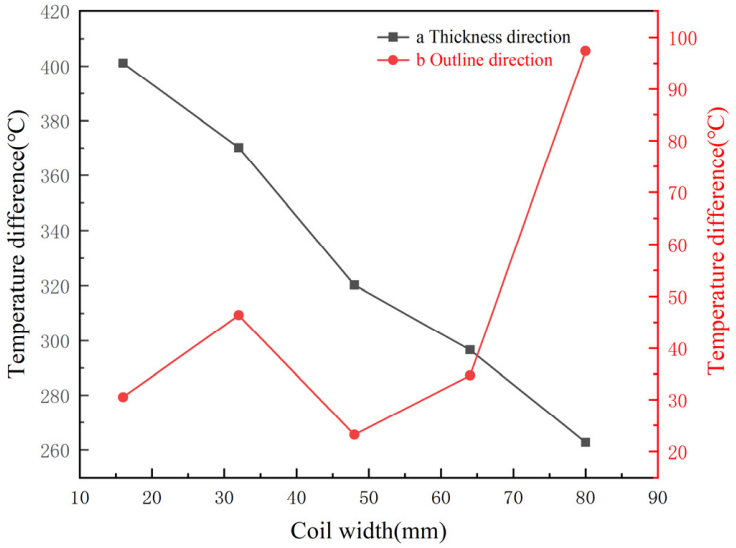


Figure 17. The variation of cam temperature difference under different induction coil widths.

4.4. Process Optimization

4.4.1. Presentation of Equivalent Parameters

In order to optimize the heating process, help determine the best parameter combination, and achieve uniform distribution of heating temperature, the equivalent relationship between temperature and other parameters is proposed. The moving speed v, the width of the induction coil h, the gap s, and the coordinate x of the cam thickness direction are set as independent variables, and the temperature T is set as the dependent variable. The correlation equation between the temperature and the four independent variables is fitted using linear and polynomial fitting methods.

In this section, based on the dynamic induction heating simulation model, the temperature results in the cam thickness direction for different factors are fitted. Firstly, linear and polynomial fits are performed for 12 different speeds and 5 x values, a total of 60 data sets.

The temperature at various locations along the cam's thickness direction and the x-axis coordinate are shown to be related as follows:

$$T_1 = A + Bx \tag{20}$$

where A and B are equations about velocity v, and x is the x-axis coordinate of the cam thickness direction.

$$A = 1471.09898 + 27.93355v - 7.55536v^2 + 0.3884v^3 \tag{21}$$

$$B = -32.16512 + 16.71312v - 4.08085v^2 + 0.47168v^3 - 0.02557v^4 + 5.22532e^{-4}v^5 \quad (22)$$

The independent variable induction coil width h is introduced. A total of 25 sets of data for 5 kinds of induction coil widths and 5 x values are fitted by linear and polynomial fitting.

$$\Delta T_1 = C + Dh \quad (23)$$

where C and D are equations about the independent variable x.

$$C = 722.23229 - 0.89066x - 0.02298x^2 \quad (24)$$

$$D = -10.85333 - 0.02823x + 0.0024x^2 - 222524e^{-5}x^3 \quad (25)$$

The independent variable gap s is introduced. Four hundred data sets are fitted for 8 gaps and 5 x values using both polynomial and linear fitting techniques.

$$T_2 = E + Fx \quad (26)$$

where E and F are equations about the independent variable gap s.

$$E = 1457.07333 - 9.73167s \quad (27)$$

$$F = 23.64366 - 26.07654\mathrm{s} + 9.07993\mathrm{s}^2 - 1.50965s^3 + 0.12023s^4 - 0.00369s^5 \quad (28)$$

$$\Delta T_2 = T_2(s, x) - T_2(5, x) \quad (29)$$

Combine the above independent variable equations to form a new equation.

$$T(x, v, h, s) = T_1(x, v) + \Delta T_1(x, h) + \Delta T_2(x, s) \quad (30)$$

Based on the above equations, the temperature difference δ of the cam in the thickness direction can be predicted, which provides a reference for the uniformity analysis of the temperature distribution during the dynamic induction heating process.

$$\delta = \mathrm{k}_0(T_{max} - T_{min}) \quad (31)$$

where T_{max} is the maximum value of temperature in the cam thickness direction, T_{min} is the minimum value of temperature in the cam thickness direction, and k_0 is the equation coefficient of 0.94.

4.4.2. Temperature Field Prediction

The equivalent parameter δ is used to predict the temperature difference in the thickness direction of the cam under different parameters, and compared with the dynamic induction heating simulation results under different factors in Section 4.3. Figure 18 shows the comparison between the predicted and simulated results for the equivalent parameter δ. From the figure, it can be seen that the simulated results are consistent with the predicted results.

According to the prediction results and simulation results, the correlation coefficient of temperature difference in the thickness direction is R^2 = 0.994497. The closer R^2 is to 1, the better the fit. The results show that the equivalent parameter δ can be used as a method to predict the temperature uniformity in the thickness direction of the cam.

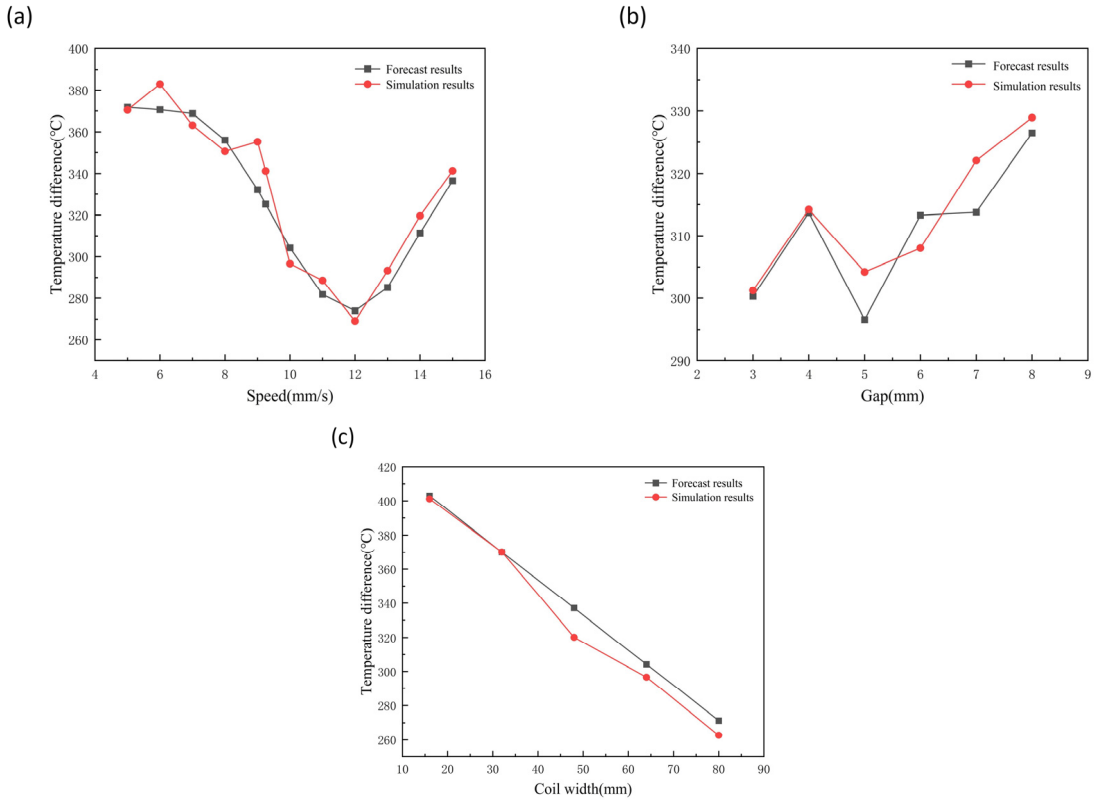


Figure 18. Comparison of simulated and predicted temperature differences, (**a**) moving speed (**b**) gap between the induction coil and the workpiece (**c**) induction coil width.

In order to select the best process parameters, the best temperature uniformity is obtained. In this paper, a three-variable orthogonal test is established, and the ANOVA method is used to analyze the significance of moving speed, gap, and induction coil width. Thus obtaining the optimum process combination. In this paper, three-factor levels are set for each variable impact factor. As shown in Table 3. At the same time, the orthogonal design Table 4 was established.

Table 3. Parameter level record.

Factor Levels	Moving Speed (mm/s)	Gap (mm)	Induction Coil Width (mm)
1	10	5	64
2	12	6	48
3	14	7	32

Table 4. Orthogonal test array.

Serial Number	Factor 1	Factor 2	Factor 3	Temperature Difference (°C)
1	1	1	1	296.6
2	1	2	2	329.7
3	1	3	3	364.5
4	2	1	3	342.65
5	2	2	1	286.5
6	2	3	2	309.9
7	3	1	2	348.8
8	3	2	3	409.8
9	3	3	1	346.3

It can be seen from Table 5 that the three-factor analysis of variance is used to study the influence of Moving speed, Gap, and Induction coil width on Temperature difference. It can be seen from the above table that Moving speed shows significance (F = 68.504, $p = 0.014 < 0.05$), indicating that the main effect exists, and Moving speed will have a different relationship with Temperature difference. Gap did not show a significant difference (F = 4.028, $p = 0.199 > 0.05$), indicating that Gap does not have a differential relationship with Temperature difference (°C). Induction coil width (mm) showed a significant difference (F = 87.403, $p = 0.011 < 0.05$), indicating that the main effect exists. Induction coil width (mm) will have a different relationship with Temperature difference (°C). Therefore, it is found that the primary and secondary order of the three factors affecting the temperature difference is: induction coil width, moving speed, and gap.

Table 5. Three-factor analysis of variance results.

Source of Variance	Quadratic Sum	df	Mean Square	F	*p*
Intercept	1023267	1	1023267	29190.8	0.000 **
Moving speed (mm/s)	4802.762	2	2401.381	68.504	0.014 *
Gap (mm)	282.376	2	141.188	4.028	0.199
Induction coil width (mm)	6127.722	2	3063.861	87.403	0.011 *
Residual	70.109	2	35.054		

R^2: 0.994. * $p < 0.05$ ** $p < 0.01$.

According to Table 6, the results of multiple comparisons after the analysis of factor 1 moving speed: when the moving speed is 12 mm/s, the *t*-test corresponds to the minimum *p*-value at this time, indicating that the difference between the two is the most significant. The specific mean difference is −55.3, indicating that the average temperature difference corresponding to 12 mm/s is lower than the average temperature difference corresponding to 14 mm/s. Therefore, the corresponding temperature difference is the smallest when the moving speed is 12 mm/s. Similarly, it can be seen from Tables 7 and 8 that when the gap is 5 mm, the corresponding temperature difference is the smallest. When the width of the induction coil is 64 mm, the corresponding temperature difference is the smallest. In summary, the optimum process parameters of temperature uniformity in the induction heating process can be obtained: the moving speed is 12 mm/s, the gap is 5 mm, and the width of the induction coil is 64 mm.

Table 6. Post hoc multiple comparisons (Moving speed (mm/s)).

Item	Mean Difference	Standard Error	*t*	*p*
10.0–12.0	17.267	4.834	3.572	0.070
10.0–14.0	−38.033	4.834	−7.868	0.016
12.0–14.0	−55.300	4.834	−11.439	0.008

Table 7. Post hoc multiple comparisons (Gap (mm)).

Item	Mean Difference	Standard Error	*t*	*p*
5.0–6.0	−12.667	4.834	−2.620	0.120
5.0–7.0	−10.900	4.834	−2.255	0.153
6.0–7.0	1.767	4.834	0.365	0.750

Table 8. Post hoc multiple comparisons (Induction coil width (mm)).

Item	Mean Difference	Standard Error	*t*	*p*
32.0–48.0	42.833	4.834	8.860	0.012
32.0–64.0	62.500	4.834	12.929	0.006
48.0–64.0	19.667	4.834	4.068	0.055

The accuracy of finite element modeling results has been verified by scholars through a large body of work [4,32]. Bao L [10] and Zhao Y [21] compared the temperature distributions of steel plates and bevel gears during induction heating in simulation and experiment, respectively, and the simulation results were consistent with the experimental results. In Reference [38], the linear and nonlinear fitting methods of Origin 2022 software are introduced in detail, and experimental verification is carried out to prove the accuracy of Origin software fitting. The feasibility of multivariate linear and nonlinear fitting in the induction heating process was explored and experimentally verified by Jinsong Bai [39] and Fengsheng Sun [40]. The prediction results of this paper are consistent with the simulation results, so it can be considered that the conclusions are accurate. It can provide the corresponding reference for subsequent research.

5. Conclusions

In this paper, an electromagnetic-thermal multi-physical field coupling model is established to analyze the temperature distribution law of the cam during induction heating. Compared with static induction heating, the influence of different factors on the temperature distribution uniformity in the thickness direction and contour line direction of the cam under dynamic conditions is studied.

(1) Induction heating under dynamic conditions can reduce the problem of excessive temperature in the middle of the workpiece under static conditions, and can effectively improve the temperature uniformity and heating rate in the contour line direction.
(2) The temperature in the thickness direction of the cam is significantly impacted by the end effect when the movement speed is less than 12 mm/s. The end impact is lessened and temperature uniformity is enhanced as moving speed increases. When the movement speed exceeds 12 mm/s, moving too quickly can easily result in a too-short residence period in the heating area, which can reduce the temperature uniformity by affecting the temperature distribution uniformity. In the direction of the cam contour line, the uniformity of temperature decreases with the increase in speed. A suitable rise in velocity contributes to the enhancement of the cam's overall homogeneous temperature distribution.
(3) When the gap between the induction coil and the workpiece is small, the electromagnetic field distribution is more concentrated, and the local heating rate is too fast, resulting in uneven temperature distribution in the thickness direction of the cam. Increasing the gap can improve the temperature uniformity, but too large a gap can easily lead to a decrease in electromagnetic field strength and temperature uniformity.
(4) Increasing the width of the induction coil can effectively improve the distribution of the electromagnetic field in the thickness direction of the cam, reduce the influence of the end effect, and make the overall heating more uniform. In the direction of the cam contour, as the width of the induction coil increases, the uniformity of the temperature decreases. It provides a corresponding reference for the design of the coil.
(5) The equivalent parameter δ is presented to describe the temperature uniformity change in the thickness direction of the cam during dynamic induction heating under different factors. It can effectively predict the temperature of the cam thickness direction, optimize the heating process, and guide the selection of cam induction heating process parameters.

Author Contributions: Conceptualization, X.S. and K.W.; methodology, X.S., G.L. and L.Z.; software, K.W., G.L. and C.L.; validation, K.W. and C.L.; formal analysis, X.S.; investigation, J.C., L.S. and H.W.; resources, L.Z.; data curation, J.C., L.S. and H.W.; writing—original draft preparation, X.S. and K.W.; writing—review and editing, X.S., K.W. and L.Z.; supervision, X.S. and L.Z.; project administration, X.S.; funding acquisition, L.Z. All authors have read and agreed to the published version of the manuscript.

Funding: This research was supported by the High-tech Ship Research Project (CBG5N21-2-2), the General project of natural science research of Institutions of Higher Education of Jiangsu Province of China (21KJB510016) and the National Natural Science Foundation of China (62203193).

Institutional Review Board Statement: Not applicable.

Informed Consent Statement: Not applicable.

Data Availability Statement: The original contributions presented in the study are included in the article, further inquiries can be directed to the corresponding author.

Conflicts of Interest: The authors declare that the research was conducted in the absence of any commercial or financial relationships that could be construed as a potential conflict of interest.

References

1. Skalomenos, K.A.; Kurata, M.; Shimada, H.; Nishiyama, M. Use of induction-heating in steel structures: Material properties and novel brace design. *J. Constr. Steel Res.* **2018**, *148*, 112–123. [CrossRef]
2. Díaz Moreno, J.M.; García Vázquez, C.; González Montesinos, M.T.; Ortegón Gallego, F.; Viglialoro, G. Industrial Steel Heat Treating: Numerical Simulation of Induction Heating and Aquaquenching Cooling with Mechanical Effects. *Mathematics* **2021**, *9*, 1203. [CrossRef]
3. Areitioaurtena, M.; Segurajauregi, U.; Fisk, M.; Cabello, M.J.; Ukar, E. Numerical and experimental investigation of residual stresses during the induction hardening of 42CrMo4 steel. *Eur. J. Mech. A Solids* **2022**, *96*, 104766. [CrossRef]
4. Wen, H.; Han, Y. Study on mobile induction heating process of internal gear rings for wind power generation. *Appl. Therm. Eng.* **2017**, *112*, 507–515. [CrossRef]
5. Leitner, M.; Aigner, R.; Gruen, F. Numerical Fatigue Analysis of Induction-Hardened and Mechanically Post-Treated Steel Components. *Machines* **2019**, *7*, 1. [CrossRef]
6. Tong, D.; Gu, J.; Totten, E.G. Numerical simulation of induction hardening of a cylindrical part based on multi-physics coupling. *Model. Simul. Mater. Sci. Eng.* **2017**, *25*, 035009. [CrossRef]
7. Choi, J.K.; Park, K.S.; Lee, S.S. Prediction of High-Frequency Induction Hardening Depth of an AISI 1045 Specimen by Finite Element Analysis and Experiments. *Int. J. Precis. Eng. Manuf.* **2018**, *19*, 1821–1827. [CrossRef]
8. Gao, K.; Wang, Z.; Qin, X.P.; Zhu, S.X. Numerical analysis of 3D spot continual induction hardening on curved surface of AISI 1045 steel. *J. Cent. South Univ.* **2016**, *23*, 1152–1162. [CrossRef]
9. Li, H.P.; Sun, Y.; He, L.F.; Li, Z.C. Failure analysis of ball screw in the progressive induction hardening and finishing machining. *Eng. Fail. Anal.* **2023**, *151*, 107410. [CrossRef]
10. Bao, L.; Wang, B.; You, X.; Li, H.; Gu, Y.; Liu, W. Numerical and experimental research on localized induction heating process for hot stamping steel heets. *Int. J. Heat Mass Transf.* **2020**, *1511*, 19422–119422.
11. Li, H.; He, L.; Gai, K.; Jiang, R.; Zhang, C.; Li, M. Numerical simulation and experimental investigation on the induction hardening of a ball screw. *Mater. Des.* **2015**, *87*, 863–876. [CrossRef]
12. Fisk, M.; Lindgren, L.E.; Datchary, W.; Deshmukh, V. Modelling of induction hardening in low alloy steels. *Finite Elem. Anal. Des.* **2018**, *144*, 61–75. [CrossRef]
13. Peng, W.; Chen, X.; Zhang, L.; Li, X.; Sun, J.; Zhang, D. Finite element analysis of temperature uniformity in transverse induction heating process in ESP rolling. *Int. J. Adv. Manuf. Technol.* **2021**, *115*, 3423–3439. [CrossRef]
14. Yu, C.; Xiao, H.; Qi, Z.C.; Zhao, Y.P. Finite Element Analysis and Experiment on Induction Heating Process of Slab Continuous Casting-direct Rolling. *Min. Miner.* **2019**, *116*, 403. [CrossRef]
15. Wu, Y.; Guo, X.; Yu, H.; Zhong, X.; Liu, Z.; Long, K. Homogeneous single-coil induction heating achieved by structure design. *Int. J. Appl. Electromagn. Mech.* **2023**, *72*, 327–341. [CrossRef]
16. Song, K.; Guan, J.; Li, K.; Liu, J. Experimental and numerical study of the effect of coil structure on induction nitriding temperature field. *Adv. Mech. Eng.* **2020**, *12*. [CrossRef]
17. Cui, P.; Zhu, W.; Ji, H.; Chen, H.; Hang, C.; Li, M. Analysis and optimization of induction heating processes by focusing the inner magnetism of the coil. *Appl. Energy* **2022**, *321*, 119316. [CrossRef]
18. Hömberg, D.; Liu, Q.; Montalvo-Urquizo, J.; Nadolski, D.; Petzold, T.; Schmidt, A.; Schulz, A. Simulation of multi-frequency-induction-hardening including phase transitions and mechanical effects. *Finite Elem. Anal. Des.* **2016**, *121*, 86–100. [CrossRef]
19. Sun, Y.; He, L.; Li, Z.; Li, H. Optimization of Induction Hardening for Sprocket Based on Numerical Simulation and Experiment Design. *J. Mater. Eng. Perform.* **2022**, *32*, 4338–4351. [CrossRef]

20. Barglik, J.; Ducki, K.; Kuc, D.; Smagór, A.; Smalcerz, A. Hardness and microstructure distributions in gear wheels made of steel AISI 4340 after consecutive dual frequency induction hardening. *Int. J. Appl. Electromagn. Mech.* **2020**, *63*, S131–S140. [CrossRef]
21. Zhao, Y.; Han, Y.; Xiao, Y. An asynchronous dual-frequency induction heating process for bevel gears. *Appl. Therm. Eng.* **2020**, *169*, 114981. [CrossRef]
22. Li, F.; Li, X.; Qin, X.; Rong, Y.K. Study on the plane induction heating process strengthened by magnetic flux concentrator based on response surface methodology. *J. Mech. Sci. Technol.* **2018**, *32*, 2347–2356. [CrossRef]
23. Gao, K.; Qin, X. Effect of feed path on the spot continual induction hardening for different curved surfaces of AISI 1045 steel. *Int. Commun. Heat Mass Transf.* **2020**, *115*, 104632. [CrossRef]
24. Saputro, I.E.; Chen, C.P.; Jheng, Y.S.; Huang, H.C.; Fuh, Y.K. Mobile Induction Heat Treatment of Large-Sized Spur Gear-The Effect of Scanning Speed and Air Gap on the Uniformity of Hardened Depth and Mechanical Properties. *Steel Res. Int.* **2023**, *94*, 2200261. [CrossRef]
25. Wen, H.; Xiao, Y.; Han, Y.; Zhao, Y.; Wang, S. Research on Scanning Induction Heating Process of Wind Turbine Gear: Dynamic Evolution of End Temperature. *Int. J. Precis. Eng. Manuf.-Green Technol.* **2022**, *10*, 509–520. [CrossRef]
26. Zhu, Y.; Xu, G.; Xu, C.; Li, X.; Zhou, K.; Chen, Y. Hot cracks in camshaft casting: Initiation and propagation. *Int. J. Cast Met. Res.* **2024**, *37*, 48–70. [CrossRef]
27. Sun, S.; Gong, X.; Xu, X. Research on the Bending Fatigue Property of Quenched Crankshaft Based on the Multi-Physics Coupling Numerical Simulation Approaches and the KBM Model. *Metals* **2022**, *12*, 1007.
28. Shi, X.; Lv, C.; Li, G.; Wang, K.; Chen, J.; Tang, J. Study on induction hardening performance of 34CrNi3MoA steel crankshaft. *Front. Mater.* **2023**, *10*, 1240087. [CrossRef]
29. Didi, I.; Andy, T. Induction Heating Process Design Using COMSOL®Multiphysics Software. *TELKOMNIKA (Telecommun. Comput. Electron. Control)* **2011**, *9*, 327.
30. Matúš, O.; Dobroslav, K. Simulation model of induction heating in comsol multiphysics. *Acta Electrotech. Et Inform.* **2015**, *15*, 29–33.
31. Kennedy, M.; Shahid, A.; Jon Arne, B.; Ragnhild, E.A. Analytical and Experimental Validation of Electromagnetic Simulations Using COMSOL®, re Inductance, Induction Heating and Magnetic Fields. In Proceedings of the COMSOL Users Conference, Stuttgart, Germany, 26–28 October 2011.
32. Saputro, I.E.; Chiang, C.P.; Huang, H.C.; Fuh, Y.K. Origin of non-uniform tooth flank hardening distribution in SCM440 mobile induction heat–treated steel spur gears—A parametrical study with experimental–numerical coupled investigation. *Int. J. Adv. Manuf. Technol.* **2023**, *130*, 2915–2938. [CrossRef]
33. Li, F.; Ning, J.; Liang, S. Analytical Modeling of the Temperature Using Uniform Moving Heat Source in Planar Induction Heating Process. *Appl. Sci.* **2019**, *9*, 1445. [CrossRef]
34. Tong, D.; Gu, J.; Totten, E.G. Numerical investigation of asynchronous dual-frequency induction hardening of spur gear. *Int. J. Mech. Sci.* **2018**, *142–143*, 1–9. [CrossRef]
35. Mekky, A.B.H. Computational Modelling for Specific Heat and Thermal Conductivity of Austenitic Stainless Steels Alloys at Solid Phase. *Rev. Des Compos. Et Des Matériaux Avancés-J. Compos. Adv. Mater.* **2020**, *30*, 23–27. [CrossRef]
36. Dai, S.J.; Yu, W.A.N.G.; Feng, C.H.E.N.; Yu, X.Q.; Zhang, Y.F. Design of new biomedical titanium alloy based on d-electron alloy design theory and JMatPro software. *Trans. Nonferrous Met. Soc. China* **2013**, *23*, 3027–3032. [CrossRef]
37. Park, J.; Lee, S.; Kang, S.; Jeon, J.; Lee, S.H.; Kim, H.K.; Choi, H. Complex effects of alloy composition and porosity on the phase transformations and mechanical properties of powder metallurgy steels. *Powder Technol.* **2015**, *284*, 459–466. [CrossRef]
38. Lin, X.; Yang, W.; Yu, L.; Zhang, C. Application of Origin software in experimental data and graph processing. *Sci. Technol. Perspect.* **2014**, *13*, 54–55. [CrossRef]
39. Bo, J. *Research on Deformation Law of Induction Heating Steel Plate*; Dalian University of Technology: Dalian, China, 2006.
40. Sun, F. *Local Finite Element and Experimental Regression Analysis of Induction Heating of Steel Plate*; Dalian University of Technology: Dalian, China, 2005.

Disclaimer/Publisher's Note: The statements, opinions and data contained in all publications are solely those of the individual author(s) and contributor(s) and not of MDPI and/or the editor(s). MDPI and/or the editor(s) disclaim responsibility for any injury to people or property resulting from any ideas, methods, instructions or products referred to in the content.